Ca2+ and Ag+ orient low-molecular weight amphiphile self-assembly into “nano-fishnet” fibrillar hydrogels with unusual β-sheet-like raft domains

Alexandre Poirier, Patrick Le Griel, Ingo Hoffmann, Javier Perez, Petra Pernot, Jérôme Fresnais, Niki Baccile

Self-assembled fibrillar network (SAFiN) hydrogels with β-sheet-like raft domains: Structure

Alexandre Poirier,[a] Patrick Le Griel,[a] Ingo Hoffmann,[b] Javier Perez,[c] Petra Pernot,[d] Jérôme Fresnais,[e] Niki Baccile[a,*]

[a] Sorbonne Université, Centre National de la Recherche Scientifique, Laboratoire de Chimie de la Matière Condensée de Paris, LCMCP, F-75005 Paris, France

[b] Institut Laue-Langevin, 38042 Grenoble, France

[c] Synchrotron Soleil, L'Orme des Merisiers, Saint-Aubin, BP48, 91192 Gif-sur-Yvette Cedex, France

[d] ESRF – The European Synchrotron, CS40220, 38043 Grenoble, France

[e] Sorbonne Université, CNRS, Laboratoire de Physico-chimie des Électrolytes et Nanosystèmes Interfaciaux, PHENIX - UMR 8234, F-75252, Paris Cedex 05, France

* Corresponding author:
Dr. Niki Baccile
E-mail address: niki.baccile@sorbonne-universite.fr
Phone: +33 1 44 27 56 77

Abstract

Low-molecular weight gelators (LMWG) are small molecules (Mw < ~1 kDa), which form self-assembled fibrillar networks (SAFiN) hydrogels in water triggered by an external stimulus, generally temperature but also pH, free ions or light. The great majority of SAFiN gels is described by an entangled network of self-assembled fibers, in analogy to a polymer in a good solvent. In some rare cases, a combination of attractive Van der Waals and repulsive electrostatic forces drives the formation of bundles, that is a columnar arrangement of the fibers, having a suprafibrillar hexagonal order. In this work, an unexpected micelle-to-fiber transition is triggered by Ca^{2+} or Ag^{+} ions added to a micellar solution of a novel glycolipid surfactant, whereas salt-induced fibrillation is not common for surfactants. Furthermore, the resulting SAFiN, which displays immediate hydrogel formation from about 0.5 wt%, has a so-called "nano-fishnet" structure, characterized by a fibrous network of both entangled fibers and β-sheets-like raft domains, generally observed for silk fibroin, actin hydrogels or mineral

imogolite nanotubes, but not known for SAFiN. The β-sheets-like domains, characterized by a combination of cryo-TEM and SAXS, contribute to the stability of the glycolipid gels. Furthermore, the glycolipid is obtained by fermentation from natural resources, like glucose and rapeseed oil, thus showing that naturally-engineered compounds can have unprecedented properties, when compared to the wide range of chemically derived amphiphiles.

Introduction

Water thickening in hydrogels is generally produced by an entangled fibrous network of polymers, chemically or physically cross-linked,[1,2] giving rise to widespread consumer products.[3] To improve the biocompatibility, biopolymer-based hydrogels became a source of interest and a number of studies nowadays exist in this field.[4] However, the gelling process by polymers is often irreversible, reason why low molecular weight gelators (LMWG) are developed, for they combine a fascinating self-assembly behavior, driven by non-covalent interactions, and a supramolecular assembly process, which can be tuned[5–8] more or less reversibly to form a gel.[9–11] However, may they be polymeric or self-assembled fibrillar networks (SAFiN), physical gels share the same entangled fibrillar structure.

More peculiar, some biopolymers, like silk fibroin[12–15] or actin[16–18], have a more complex hydrogel structure, where entanglement coexists with crystalline β-sheet domains, and these constituting junctions of the intertwined fibrillar network, sometimes referred to as "nano-fishnets".[12–18] β-sheets, stabilized by a combination of hydrophobic effect and inter-chain hydrogen bonding, provide an important element of structural stability of the gel,[13] of which the network elasticity is related to β-sheet junctions.[12–18] Silk fibroin gels, for instance, are irreversible and stable against temperature,[19] and can only be disassembled with highly concentrated solutions of lithium thiocyanate.

Hydrogels having "nano-fishnet", or β-sheet-like, structures, are not classical for SAFiN. Generally described as physically entangled networks, the typical X-ray or neutron scattering profile is characterized by the lone form factor of the fibers[20–24] (a more extensive list of references is given in Table S 1). In some rare cases, fibers with a homogeneous distribution of charges around their cross-section show bundling into a columnar phase with hexagonal order (Table S 1)[25,26] but SAFiN hydrogels with a β-sheet-like structure are quite unique. To the best of our knowledge, Weingarten *et al*. were one of the few, if not the only ones, showing a lamellar supramolecular arrangement of fibers composed of perylene amphiphiles.[27] However, such arrangement was not associated with the gel but rather to the

colloidal structure before gelling. For this reason, this system cannot be described as a "nano-fishnet" β-sheet structure, similarly to silk fibroin hydrogels.

In this work, we report the formation of SAFiN hydrogels having a "nano-fishnet" structure, composed of entanglements and β-sheet-like rafts, similarly to silk fibroin or actin. They are entirely composed of a bolaform C18:1 glycolipid (G-C18:1), a new compound produced by microbial fermentation in the presence of rapeseed oil. This compound actually displays a rare triple surfactant-lipid-gelator nature at concentrations below 5 wt%.[28] Early studies have shown its micellar phase at basic pH and a vesicle phase below neutral pH.[29,30] However, current work[31] shows that addition of specific cations to the micellar phase under neutral-alkaline conditions of pH not only promote a cylinder/wormlike phase, expected for surfactant micelles in contact with multivalent cations,[32–35] but also an unexpected fiber phase.[31] Self-assembled fibers are generally reported for peptide-based and other low molecular weight gelators (LMWG), but not known for anionic surfactants with cations.[36–41]

The specific use of Ca^{2+} or Ag^{+} in combination with a micellar solution of G-C18:1 promotes the formation of SAFIN hydrogels,[42] with impressive stability towards shear strain at temperatures (up to 80°C), similarly to silk fibroin hydrogels,[19] well above the melting temperature of G-C18:1.[42] In this work, the combination of cryogenic transmission electron microscopy (cryo-TEM) and small-angle X-ray scattering (SAXS) demonstrates the formation of fibers, which, in the absence of external shear, organize themselves in β-sheet-like raft structures. Isothermal titration calorimetry (ITC) suggests a multiple role of the cations, supposed to coordinate the G-C18:1 molecules and drive the two-dimensional alignment of the fibers. Additional data, presented in a sister work, illustrate the mechanism of formation of G-C18:1 fibers through cation and pH-resolved *in situ* SAXS experiments.[43]

Although largely studied in the literature, LMW hydrogels share a common isotropic, entangled, arrangement of the fibers, which generally align only under shear. This work, combined with complementary data published elsewhere,[31,42,43] shows that the biobased molecules with unique functional and bolaform molecular structure can assemble into fibrous hydrogels with unprecedented β-sheet-like raft structures in a spontaneous manner without shear.

Material and methods

Chemicals. The monounsaturated glucolipid G-C18:1 (M_w = 460 g.mol^{-1}) contains a β-D-glucose unit covalently linked to oleic acid. The molecule is obtained by fermentation from of the yeast *Starmerella bombicola (ΔugtB1)* according to the protocol given before.[30,44] The

compound is purchased from the Bio Base Europe Pilot Plant, Gent, Belgium, lot N° APS F06/F07, Inv96/98/99 and used as such. NaOH (≥98wt% pellets) is purchased from Sigma Aldrich, $CaCl_2$ in pellets and liquid 35wt% HCl are purchased from VWR. $AgNO_3$ is purchased from Sigma Aldrich.

Sample preparation. G-C18:1 is dispersed in milli-Q water and the pH is adjusted by an initial addition of concentrated NaOH (5 M), followed by a refinement with few µL of more diluted NaOH (or HCl) solution (1 M, 0.5 M or 0.1 M). The targeted molecular ratio to be roughly in the region of pH 8 is [NaOH]/[G-C18:1] = 0.7-0.8. The solution is homogenized by vortexing. To form a hydrogel, a $CaCl_2$, or $AgNO_3$, solutions are prepared at 1 M and the appropriate amount is added to the G-C18:1 solution according to the molar ratio $[AgNO_3]/[G\text{-}C18:1] = 1.0$ and $[CaCl_2]/[G\text{-}C18:1] = 0.6$. Typically, for a total 1 mL volume, 62.5 µL of $AgNO_3$ (1 M), or 40 µL of $CaCl_2$ (1 M), are added to the complementary volume of 3 wt% G-C18:1. After the addition, the solution is immediately stirred during about 30 s. All samples are aged between few minutes and 3 days before any experiments. Hydrogels prepared from Ca^{2+} and Ag^{+} are respectively labeled $\{Ca^{2+}\}$G-C18:1 and $\{Ag^{+}\}$G-C18:1.

Additional information on the experimental methods and analytical techniques are given in the supporting information.

Results

Bolaform glucolipid G-C18:1 contains a free-standing carboxylic acid end-group on its alkyl chain.[28] For this reason, it behaves as a surfactant above and as a lipid below neutrality of water (pH ~7) and room temperature: a predominant micellar phase is observed at the basic pH while a vesicular phase is reported at acidic pH.[29,30] Qualitative experiments show that precipitation occurs when various sources of cations are added below neutrality, in the vesicle phase, most likely inducing the formation of a lamellar aggregate, in analogy to the effect of lowering pH below 4[45,46] and in agreement with other vesicle-cation systems.[47] On the contrary, adding alkaline earth and transition metal cations in the micellar phase above neutrality induces gelling, as shown by oscillatory rheology experiments.[31,42] Figure 1 shows the increase of G' against the G-C18:1 weight fraction, $\phi_{\text{G-C18:1}}$, at a fixed [cation]/[G-C18:1] ratio, which is optimized and discussed elsewhere.[31,42] One finds that silver hydrogels are at least one order of magnitude stronger than calcium gels. G' scales with $\phi_{\text{G-C18:1}}$ following a power law of 2.3 and 2.6 for calcium and silver hydrogels, respectively. Scaling law with a

power dependency between 2.3 and 2.6 are close to 2.25, the well-known value reported for entangled fibrils in a good solvent, according scaling theory developed by De Gennes in 1976.[48] However, similar values are also reported for nanofibrillated systems,[49] including SAFiN hydrogels.[50]

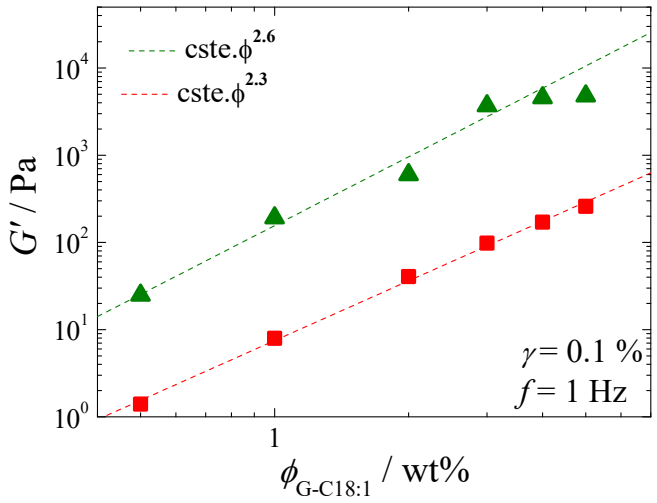

Figure 1 – Oscillatory rheology. Elastic moduli, G', of {Ca^{2+}}G-C18:1 (square) and {Ag^{+}}G-C18:1 (triangle) hydrogels at basic pH as a function of G-C18:1 weight fraction, $\varphi_{G\text{-}C18:1}$, at the molar ratio [Ca^{2+}]/[G-C18:1]= 0.6 and [Ag^{+}]/[G-C18:1]= 1. The dash lines correspond to a linear power law fitting. Additional data and corresponding frequency and strain sweep profiles are given in Ref. [42].

Gelling of glucolipid G-C18:1 is unexpected. Its known phase behavior[29,30] cannot explain its gelling properties. Considering its tendency to form interdigitated membranes at pH below 7, one could suppose the formation of vesicle gels,[51] or even a lamellar gel,[52] in analogy with the gelling properties of a similar glucolipid with a saturated fatty acid.[53] A simplistic understanding of the cations effect on self-assembly, well known in the literature,[37,40,54,55] could suppose neutralization of the negative charges of G-C18:1. Consequent variation in the lipid packing parameter could lead to the formation of either defective membranes, responsible for gelling in lipid lamellar systems,[52,53] or elongated (cylinder or wormlike) micelles.[32–35,41,56–58] However, a combination of cryo-TEM and SAXS experiments do not corroborate these hypotheses.

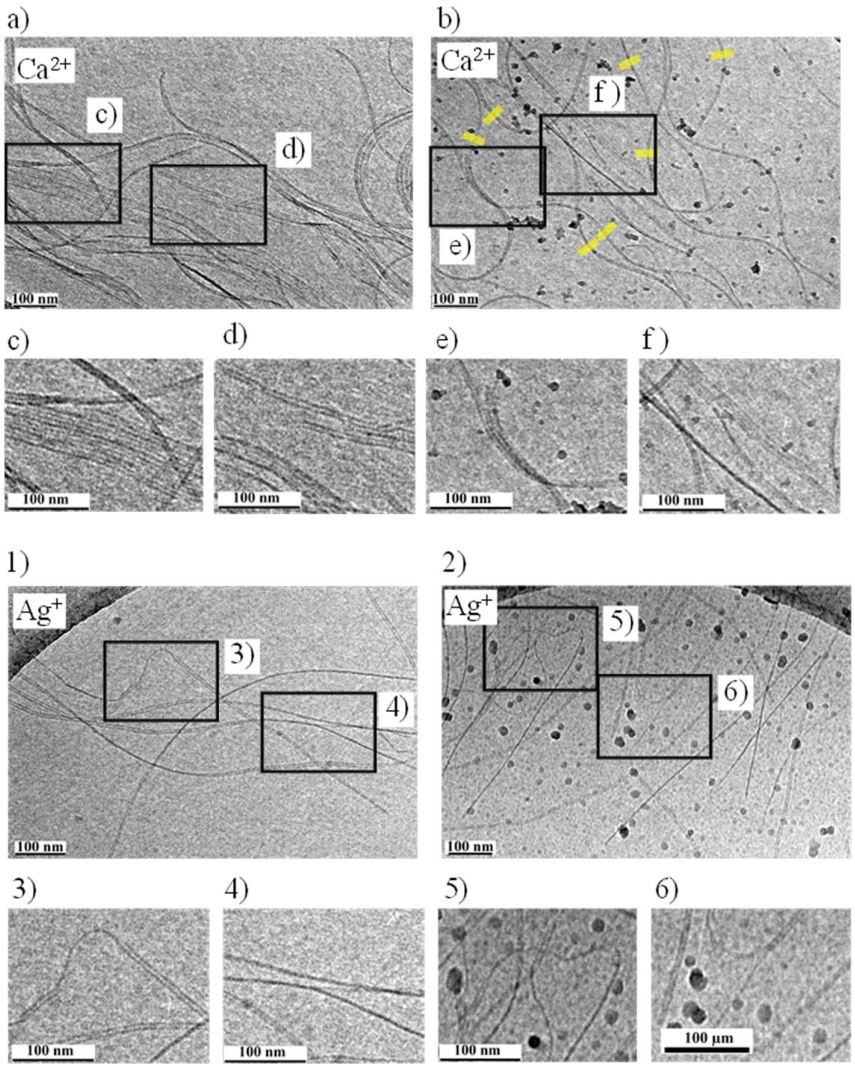

Figure 2 - Cryo-TEM images of 0.5 wt% G-C18:1 at a ratio [Ca^{2+}]/[G-C18:1] = 0.6 (a-f), [Ag^{+}]/[G-C18:1] = 1 (1-6) in water at a basic pH. Samples are not sheared. In a,b) and 1,2) black rectangles indicate magnified regions of interest. a) Large ordered rafts, magnified in c, d). b) Free fibrils locally assembled into dimeric or trimeric rafts. Yellow lines are used to measure the fiber's cross section, 10.3 ± 0.8 nm. Magnified picture e,f) show local and small rafts. 1,2) Silver fibrils locally self-assemble in small dimeric rafts, magnified in 3-6).

Cryo-TEM (Figure 2) and SAXS (Figure 3) of {Ca^{2+}}G-C18:1 and {Ag^{+}}G-C18:1 hydrogels invalidate the lamellar and micellar hypotheses in favor of a fibrillar phase, never reported before for this compound and actually not expected for surfactant solutions in the presence of mono or multivalent cations (for a broader literature survey, refer to ref. [31]). Previous cryo-TEM and SAXS analysis of a salt free G-C18:1 solution show either free micelles, membranes or vesicles at pH above 8, around 7 and below 7, respectively.[29]

Free fibers (Figure 2, panels b and 1) but also fiber di/trimers (Figure 2, panels e,f and 3-6) and even β-sheet-like rafts (Figure 2a,c,d) are observed throughout the sample, both for

{Ca^{2+}}G-C18:1 and {Ag^{+}}G-C18:1 hydrogels. The width of the individual fiber is estimated to about 10 ± 1 nm for {Ca^{2+}}G-C18:1 and 5 ± 1 for {Ag^{+}}G-C18:1. As far as the morphology is concerned, cryo-TEM may erroneously suggest the presence of nanotubes. However, a more attentive observation shows that what look like nanotubes (e.g., Figure 2d) are in fact an association of individual fibers over hundreds of nanometers, or even micron, scale. This is particularly clear on Figure 2, panels 3-6 for the {Ag^{+}}G-C18:1: individual fibers merge at a given point in space and are associated for their entire length. Figure 2, panel 3 nicely shows how a single flexible fiber connects two other individual fibers and their extremities: cryo-TEM then suggests specific attractive side-by-side interactions between the fibers, spontaneously occurring in water in the absence of shearing. Interactions, of which the possible driving force is discussed later, occur on length scales of tens of nanometers and are characterized by the presence of large, highly ordered, rafts, recalling the β-sheet structure in silk fibroin[12–15] or actin[16–18] gels. If aggregation into hexagonally packed bundles has been spuriously reported for charged fibers,[25,26] β-sheet-like rafts, otherwise common in mineral imogolite (mineral aluminosilicates) nanotube systems,[59] are in fact extremely rare for SAFiN[27] and, to the best of our knowledge, never reported for SAFiN hydrogels.

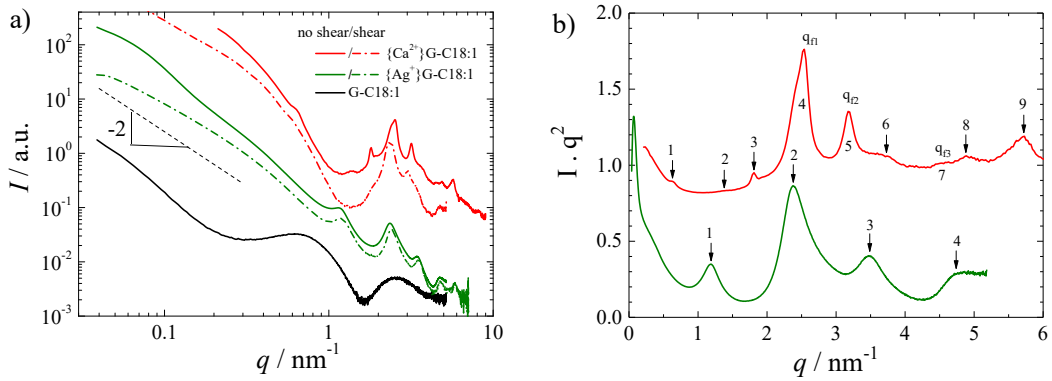

Figure 3 - SAXS profiles of a) 2 wt% of G-C18:1 in water at a basic pH (pH 8) in the absence (black) and presence of Ca^{2+} (red) and Ag^{+} (green). Segmented lines: sheared gels; straight lines: static gels. b) Kratky plots of static gels in a). Peaks are listed in Table S 2 of the supporting information.

Both the fibrillar structure and massive supra-fibrillar organization in bulk are confirmed by SAXS (Figure 3). The overall signal of the ion-free liquid G-C18:1 solution at basic pH (black line, Figure 3a) is consistent with the coexistence of two or more species, attributed to micelles and flat membranes during the pH-induced micelles-to-vesicle transition for this sample in the pH range between 7 and 8.[29,30] The broad hump centered at about 0.8 nm^{-1} and the oscillation above 1 nm^{-1} are characteristics of repulsive electrostatic interaction and

micellar morphology, respectively. The strong low-q scattering, with log(I)-log(q) dependency of about -2, is typical for flat structures, identified before as membranes.[29,30] When a gel forms by adding the appropriate amount of Ca^{2+} (or Ag^{+}), the micelle signal is replaced by a more complex scattering profile having a -2 dependency of the intensity below 0.4 nm^{-1} and a series of diffraction peaks above 0.5 nm^{-1} and attributed to a long-range structural order.

All {Ag^{+}}G-C18:1 gels have the same profile, independently of the G-C18:1 concentration (Figure S 1b), content of Ag^{+} or shearing (Figure 3a). Four broad peaks at a ratio of 1:2:3:4 (Figure 3b, Table S 2b) identify a lamellar order. Since cryo-TEM excludes any flat lamellar phase, as previously observed for analogous compounds,[29] and it only shows individual fibers and their raft-like aggregation, the lamellar order can only be explained by the side-by-side association of the fibers. The first peak is systematically observed at 1.18 nm^{-1}, corresponding to a repeating distance of 5.32 nm, which includes the fiber's cross section and interfiber water layer. The latter is estimated to few Å according to cryo-TEM, that is in the range of the primary hydration force counter balancing attractive force of Van der Waals contributions between fibers.[60] A fiber's cross-section in the order of 5 nm is then in good agreement with the qualitative estimation of the fibers' size by cryo-TEM. The low-q slope of the SAXS profiles corresponding to this set of samples is hard to evaluate due to the superposition of two scattering signals below and above 0.1 nm^{-1}.

{Ca^{2+}}G-C18:1 gels display two systematic SAXS profiles. Sheared gels, may them be obtained by controlled shear[42] or by the simple action of introducing them in the SAXS capillary, show the same scattering-diffraction pattern, typically illustrated by the segmented red line in Figure 3a, and independently of the lipid concentration (Figure S 1a). The low-q scattering has a log(I)-log(q) dependence between -1.8 and -2, observed before for fibers with a flat cross-section,[61,62] and four diffraction peaks, which are most likely associated with the fiber's crystalline structure.

Figure S 2 shows the tentative attribution of the peaks and evaluation of the fiber's structure. First of all, one could pinpoint the main peaks at q_1= 2.41 nm^{-1}, q_2= 3.02 nm^{-1} and q_3= 4.71 nm^{-1}, identifying a ratio of q_2/q_1= 1.25 and q_3/q_1= 1.95 (~2). Many similar SAFiN systems only show one main structural peak corresponding to an inter-lipid distance,[61,62] or an hexagonal order ($1 : \sqrt{3} \equiv 1.73 : 2$) within the fiber (Table S 1). However, the peak positional ratio q_2/q_1= 1.25 found here is quite atypical. If such ratio certainly excludes any lamellar and hexagonal arrangement, as well as all cubic phases due to the strong anisotropy of the fibers, two other possibilities exist. In the first one, one could suppose a ribbon mesophase with a

rectangular, or oblique, 2D lattice orthogonal to the fiber's longitudinal axis (Figure S 2b);[63,64] in the second one, one could suppose a flat ribbon with a rectangular, or oblique, crystalline arrangement of the lipids within the fiber's plane (Figure S 2a).[65,66] The values of calculated wavevectors, q(calc), match well the experimental data, q(exp), as shown in Figure S 2b, when a 2D rectangular/oblique lattice with (h,k)= 1,0; 0,1; 1,1; 0,2 is employed. However, the rectangular lattice (γ= 90°, hypothesis (A) in Figure S 2b) requires indexing the broad shoulder at 1.8 nm^{-1} as the (1,0) plane. Although not impossible, this hypothesis seems to be inconsistent when considering the peak width, much broader for (1,0) than for all other reflections. On the contrary, the use of an oblique lattice requires indexing of the multicomposite peak at about 2.40 nm^{-1} (hypothesis (B) in Figure S 2b). For this hypothesis, the broad shoulders at 1.8 nm^{-1} and 3.5 nm^{-1} could be attributed to the subjacent oscillation of the form factor. Possibly, one last hypothesis could leave room for interpreting the data as a combination of coexisting polymorphs with similar periods, as recently proposed for comparable glycolipid fibrillary hydrogels.[67,68] Finally, a broad peak is observed at 13.9 nm^{-1} (Figure S 1a), corresponding to a d-spacing of 0.45 nm, compatible with an intra-alkyl chain distance, generally poorly affected by molecular packing.[69,70] Although important, a detailed study of the crystal structure of SAFiN is a task *per se* and out of the scope of this work.

{Ca^{2+}}G-C18:1 gels at rest generate a scattering profile with a similar low-q slope (-2) but a richer diffraction pattern than the one commented above. A series of additional peaks, starting at q= 0.62 nm^{-1} superpose to the pattern corresponding to the fiber's structure. Indexed from 1 through 9 in the Kratky plot in Figure 3b, they strongly suggest a lamellar order, fully listed in Table S 2a. The peak at q= 0.62 nm^{-1} identifies a typical size of 10.1 nm, in good agreement with the corresponding fiber's cross section estimated by cryo-TEM, and indicating that about four G-C18:1 molecules are contained in the fiber's cross-section, as possibly illustrated in Figure S 2a,b.

The lamellar order found in SAXS for both {Ca^{2+}}G-C18:1 and {Ag^{+}}G-C18:1 gels cannot be explained by a classical 2D lamellar phase and it rather confirms the side-by-side association of fibers into β-sheet-like rafts (Figure 2), with strong similarities to the "nano-fishnet" described for silk fibroin.[15] Interestingly, the width of the SAXS peaks is not equivalent across samples. The peaks are systematically sharper for the {Ca^{2+}}G-C18:1 gels than for the {Ag^{+}}G-C18:1 gels, probably indicating that {Ca^{2+}}G-C18:1 gels are characterized by a fibrillar alignment over a longer distance. Cryo-TEM seems to corroborate this observation showing rafts composed of more than three fibers for {Ca^{2+}}G-C18:1 gels

(Figure 2c-f), while the association of only two or three fibers are generally observed for {Ag^+}G-C18:1 gels (Figure 2, panels 3-6).

The dependency of log(I)-log(q) at low scattering vectors (slope) identifies either a specific shape (-1: rod, -2: plane) but also mass (-1 / -3) and surface (-3 / -4) fractals.[71] Figure S 1c summarizes the slopes measured for the {Ca^{2+}}G-C18:1 gels analyzed by SAXS. Cylindrical fibers are expected to follow a -1 dependence, but this value is only observed under highly diluted (0.1 wt%) conditions. Upon increasing concentration, the slope systematically increases towards values close to -2, varying between -1.8 for sheared gels and -2.2 for gels at rest. Values in the order of -2 are certainly classical for nanobelts[61,72] and twisted ribbons,[73] and observed before for other glycolipids.[50,62] However, it is not reasonable to explain a concentration-dependent evolution from -1 to an approximate -2 slope by a change in fiber morphology. If an isotropic cross-section of individual fibers themselves is not excluded, and actually highly possible, one could also interpret the -2 slope as the signature of the wide presence of fiber rafts, flat in nature. {Ag^+}G-C18:1 gels display a more complex low-q scattering behavior. A crude estimation of the low-q slope shows values between -2.6 and -3, typical of mass fractals. However, a closer look at some profiles (2 wt%, 3 wt% in Figure S 1b or Figure 3) actually indicates the superposition of at least two scattering signals, making it impossible to have a correct estimate of the slope. Occasionally, the scattering profile does not appear multicomposite and typical slopes in the order of -2 can also be measured, reinforcing the hypothesis of flat fibers/rafts.

Origin of the fiber's β-sheet-like raft structure

The fibrillar hydrogels are commonly observed for a large number of systems, including biopolymers,[14] surfactants,[74] peptides[75] and peptide amphiphiles,[10] biosurfactants.[50,76] Fibrillation by mono and multivalent cations is also well known for bile salts,[77] low-molecular weight gelators,[5,78,79] peptides, peptide-derivatives[37,38,80] and polymers.[81–85] Despite the chemical and physicochemical difference between these systems, they all share a common structure-property denominator: fibrillar entanglement generates the elasticity of the hydrogels. The magnitude of the elastic modulus varies from system to system and strictly depends on the length, dispersion in size of the fiber's cross section as well as spherulite formation. The strength of SAFiN hydrogels are very sensitive to the kinetics of fiber's formation and, in this regard, to the rate of temperature[86] or pH variation,[76] solvent injection,[87] etc… If a comparison across the magnitude of elastic moduli among samples of different chemical origin is not pertinent, most systems are characterized by the absence of specific

forces driving the mutual fibers' interactions. The corresponding SAXS (or SANS) scattering profiles are characterized by the fiber's form (and possibly structure) factor (see references "SAFiN with disordered fibers" in Table S 1). Eventually, the elastic properties depend on entanglement and/or spherulite formation.[88]

In the absence of external driving forces (e.g., magnetic or electric fields, shearing), only a restricted number of known systems show some supra-fibrillar order, systematically characterized by the formation of bundles having 2D hexagonal packing (references in Table S 1). For instance, amphiphilic peptides assemble into long range hexagonal packing of fibrils in bulk solution, driven by electrostatic repulsion of the charged aminoacids in the peptide portion.[89] Less defined bundles with a hexagonal packing are also suggested for steroid derivatives.[25] Similar findings, but on microtubules, were reported by Needleman *et al.*.[90] As a general understanding, a combination between attractive Van der Waals and repulsive (short-range) hydration and/or (long-range) electrostatic forces can sometimes drive fiber bundling, generally into hexagonal lattice[90,91] (additional references in Table S 1) and rarely into lamellar dehydrated crystals.[92] Such phenomenon is also driven by di- or multivalent counterions, indicating that salt bridge-like cross-linking could be another possible, additional, driving force.[90,91] The work of Terech *et al.* is of particular interest, because it shows the gelling properties of tripodal cholamide-based molecules in relationship to their fibrillation into hexagonally ordered bundles.[25] On the other hand, one of the few, if not the only work to the best of our knowledge, exhibiting lamellar aggregation of self-assembled fibers was only reported to occur in a colloidal solution, but not in the corresponding salt-induced hydrogel.[27]

The present system shows a further level of complexity with respect to the vast majority of the literature.[28] First of all, Ca^{2+} and Ag^{+} drive an unexpected micelle-to-fiber, rather than micelle-to-vesicle or micelle-to-wormlike transition. The latter is not only expected for surfactants-cation systems, but also found for G-C18:1 either upon acidification of pH[29,30] or by employing transition metal cations with complex speciation in water.[31] Classical entanglement is not excluded but the unexpected side-by-side association of the fibers seems to play an important role in the gel strength and fibers' stability.[42] Furthermore, *in situ* rheo-SAXS experiments show that, differently than most anisotropic systems, fibers in $\{Ag^{+}\}$G-C18:1 and $\{Ca^{2+}\}$G-C18:1 do not show any shear-induced alignment up to at least 100 s^{-1}, making these hydrogels quite stable, even well above room temperature.[42]

On the basis of concentration- and shear-dependent SAXS experiments, Ca^{2+} and Ag^{+} play a slightly different role. $\{Ca^{2+}\}$G-C18:1 systematically forms crystalline fiber from low

to high concentrations (Figure S 1). They tend to associate into lamellar rafts at rest (shear/no shear profiles in Figure 3), depicting a two-step mechanism, even if the occasional signature of rafts can be observed under shear or at low concentrations. The corresponding hydrogel is less stable against temperature[42] while the rafts disassemble under shear. On the contrary, {Ag^+}G-C18:1 immediately forms fiber rafts in a single step, independently from concentration (Figure S 1) and shear (Figure 3 and Ref. [42]). Furthermore, gelation by silver occurs at lower $\varphi_{G\text{-}C18:1}$ and G' is at least ten times higher than with calcium (Figure 1), suggesting stronger interactions. This is probably explained by the coordination effect of carboxylate groups on silver ions, as also suggested by the lack of fibrillation when Na^+ is employed. Ag^+ is known to form a crystalline structure with a large number of fatty acids by complexation with their COO^-.[93] Ag^+/COO^- interaction has been described for many crystalline complexes.[94,95] However, gels formed by Ag^+/COO^- complexes have received less attention if compared to gels based on silver-nitrogen interaction or silver nanoparticles.[5] Metal ion Ag^+ is known to bridge peptides, coordinated by nitrogen[96] and bile salts.[77] Fibrous network based on Ag^+/COO^- complex can be obtained in organic solvent by solubilization at high temperature and cooling.[77] In water, polymeric gels induced by Ag^+ bridging carboxylate groups have been described, mainly for the use of silver as an antimicrobial agent.[97] A natural tripeptide was found as a ligand to form a lamellar hydrogel by Ag^+/sulfur complexation.[98]

The difference between silver and calcium on the self-assembly process of G-C18:1 is nicely corroborated by isothermal titration calorimetry (ITC) experiments, a technique usually employed to characterize the energetic interaction between active sites of molecules, proteins, or more generally binding ligands.[99] It consists in measuring the heat exchanged by a reaction during titration between a titrated molecule by a titrant one.

Figure 4b,c summarize the area per injection versus the molar ratio of the titrations for Ca^{2+} and Ag^+, respectively. For Ca^{2+}, the data are consistent with a two-sites binding model, from which the enthalpy of interaction can be extracted for the two steps of interactions, in complement with the corresponding stoichiometries (Table 1).[100] Binding is characterized by an endothermic (ΔH= 6.01 kJ/mol), typical for non-specific interactions (e.g., hydrophobic effect), and exothermic (ΔH= -11.17 kJ/mol), typical for specific interactions, process. The corresponding stoichiometric coefficients are 0.1 and 0.3, respectively, and the free energy is comparable (Table 1). For Ag^+, a classical independent model is used to fit the data, where only one strong exothermic event (ΔH= -37.12 kJ/mol) is observed during titration, with the stoichiometry of 0.5 and free energy of -25.4 kJ/mol (see Figure S 3 for raw data). ITC shows that two distinct phenomena characterize the Ca^{2+} system, of which the enthalpy of reactions

is less exothermic than for Ag^+. These results corroborate the difference in terms of structure (this work) and kinetics (Ref. [43]) observed by SAXS, and in particular the strong and immediate reactivity of the Ag^+ system.

Table 1 – Thermodynamic parameters extracted from fitting ITC data in Figure 4b,c.

Sample	Site	ΔH / kJ/mol	ΔS / J/mol	ΔG / kJ/mol	*n*
{Ca^{2+}}G-C18:1	1	6.01	117.3	-29.2	0.1
	2	-11.17	37.37	-22.4	0.3
{Ag^+}G-C18:1	-	-31.95	-22.00	-25.4	0.5

More specifically, the variation of enthalpy and stoichiometry (n_1= 0.1; n_2=0.3) seems to be a proof of a first interaction of the Ca^{2+} ions to the G-C18:1, with a secondary cooperative interaction partially hindered by the structuration observed in the fibers. Indeed, ΔH_2 (−11 kJ/mol) is in fairly good agreement with the absolute values obtained for Ca^{2+} adsorption onto alginate (-11.6 kJ/mol for Protanal H120L, Mw= 404 kDa) and low methoxy pectin (-12.1 kJ/mol).[85,101] In fact, the mechanism could be more complex, as shown by the alternate sign of enthalpy variation ($\Delta H_1 > 0$; $\Delta H_2 < 0$).

The most important non-specific endothermic process generally involved in the self-assembly of amphiphiles or polymers is generally related to the entropic gain in the release of water molecules. The mechanisms behind this phenomenon are multifold. The most important one is probably the well-known hydrophobic effect, known to drive the self-assembly of amphiphiles or polymers,[99,102,103] and actually observed for the interaction between G-C18:1 and polylysine.[45] However, a number of other phenomena are known to be endothermic, such as dehydration due to ion exchange (e.g., Na^+ against Ca^{2+}),[103] the weak binding of Ca^{2+} to lipid vesicles,[104] micelle-to-rod morphological transitions[105,106] and micellization of zwitterionic surfactants.[102] On the other hand, exothermic process are generally associated with specific interactions, some of which could characterize the self-assembly of {Ca^{2+}}G-C18:1: ligand-ion binding (e.g., Ca^{2+}-EDTA),[107] formation of ordered “egg-box” structures in pectin or alginate systems,[85,101] micelle-to-rod morphological transitions[108] and micellization of cationic surfactants.[102]

In the absence of additional data, one can safely state that the addition of calcium induces an initial endothermic, entropic, process. The initial micelle-to-fiber transition in {Ca^{2+}}G-C18:1 is certainly driven by the release of water molecules associated with two possibly coexisting phenomena, sodium-calcium ion exchange[103] and the hydrophobic effect related to the structural rearrangement of the fatty acid tails. The latter is driven by the need for two G-

C18:1 molecules to neutralize one Ca^{2+}. The second exothermic step is most likely related to ligand-ion binding[103,107] driven by the proximity between COO^- and Ca^{2+} inside, but also across the fibers, in analogy to the "egg-box" structures.[85,101] The cryo-TEM (Figure 2) and SAXS (Figure 3) data reasonably corroborate the latter interpretation.

It is interesting to note that the stoichiometry is n= 0.5, instead of 1, for $\{Ag^+\}$G-C18:1, strongly suggesting a coordination of silver by two carboxylate groups, also found for other systems based on bile salts.[77] One must also depict a slightly deficient, $n_1+n_2= 0.4$, stoichiometry for $\{Ca^+\}$G-C18:1, probably explained by defective cations/carboxylates interactions. This can be altered by mixing of the sample inside the measuring cell (250 rpm), which can be a limiting factor that reduces the value of n_1, compared to the quasi-static assembly of G-C18:1 for the SAXS and rheology measurements. Finally, Figure S 3 compares two ITC titrations, which explore two ranges of molar ratio (0-0.7 and 0-1.1). The second titration implies a more rapid mixing across the stoichiometric values obtained from the former titration ($n_1= 0.1$; $n_2= 0.1$). This is in favor of the importance of the kinetics of mixture that allows a more complete interaction between calcium ions and the binding site of G-C18:1, prior to their assembly into fibers.

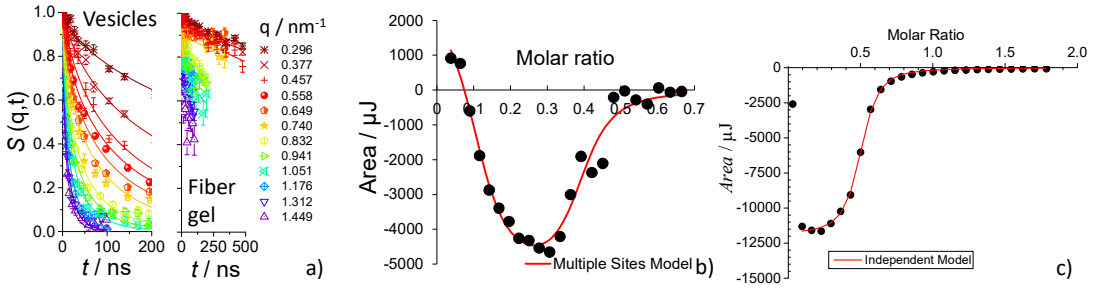

Figure 4 - a) Neutron spin-echo (NSE) experiments performed on G-C18:1 vesicles solution at 2 wt% (Ca^{2+}-free, pH 6.2) and fibrillar $\{Ca^{2+}\}$G-C18:1 gel ($[Ca^{2+}]/[G\text{-}C18:1]= 0.61$, pH 8). Normalized, *q*-dependent, spin-echo intermediate function. Data are fitted with Eq. S1. b-c) Isothermal titration calorimetry experiments performed at T= 25°C. b) Titration of a 20 mM G-C18:1 solution with 50 mM $CaCl_2$ solution. Fit (red line) is performed with a multiple site model; c) Titration of a 5 mM G-C18:1 solution with 32 mM $AgNO_3$ solution. Fit (red line) is performed with an independent model. Raw ITC data are given in Figure S 3.

Understanding the β-sheet-like structure

Although the present state of the art does not yet provide a full understanding and prediction about the effects of cations on the molecular structure and collective organization of amphiphiles in water, the abundant literature on the effects of cations on the self-assembly of amphiphiles[37,54,109] (more extensive literature survey given in Ref. [31]) could help

understanding part of our data. Calcium and silver G-C18:1 hydrogels have similar structures, equivalent gel strength,[42] resistance to temperature[42] and mechanism of formation,[43] if compared to the effect of other alkaline earth and transition metal cations.[31] As commented below, these data could be explained by the fact that the free COO^- group of G-C18:1 is a good ligand for Ca^{2+} and Ag^+.[110–112] As discussed more extensively elsewhere,[31] these cations exist as free ions in solution in the pH range the experiments are performed,[113] while most other transition metal cations, which drive a wormlike hydrogel,[31] exist in a complex mixture of hydroxylated species.[113]

Figure 5 shows the overview of the fibrillation process and β-sheet-like formation in $\{Ag^+\}$G-C18:1 and $\{Ca^{2+}\}$G-C18:1 systems.

Fibers' formation. Cation-resolved *in situ* SAXS[43] but also ITC experiments as well as negative controls using sodium ions[31] indicate a crucial role of Ag^+ and Ca^{2+} in promoting the micelle-to-fiber transition.

In the case of silver, the fiber's cross section of about 5 nm is compatible with two aligned G-C18:1 molecules. The most obvious arrangement is depicted in Figure 5b, whereas the fiber's thickness is supposed to be molecular. Silver is coordinated by the carboxylate groups,[110,113–115] as found for other fatty acid silver complexes.[93–95] Such dimeric building unit within the fibers, of which the core is rich in cations and the external sides in glucose, is actually similar to what has been reported for silver stearate[95] or bile salts.[77] The coordination reaction is highly exothermic and extremely rapid, as shown by ITC, but also by the impossibility to run silver-resolved *in situ* SAXS experiments on this system due to formation of large aggregates clogging the SAXS capillary.[43] Interestingly, the few SAXS profiles that we were able to record, and representative of a diluted silver regime, contained a random sequence of solvent (water) scattering and profiles associated to $\{Ag^+\}$G-C18:1, already characterized by the typical lamellar structure as found in Figure 3a. The same lamellar order is in fact observed even under dilute conditions (Figure S 1). Overall, the reactivity of silver towards carboxylate groups does not allow a continuous micelle-to-fiber transition, but it induces a diffusion of G-C18:1 molecules from the micelles towards the metal ions, where micelles then become a reservoir of matter, rather than nucleation sites. A similar mechanism was proposed for the pH-triggered fibrillation of C18:0 sophorolipids.[30]

In the case of calcium, the mechanism and the fiber's structure seem to be more complex. At a first stage, according to ITC and calcium-resolved *in situ* SAXS,[43] possible combination of sodium-calcium exchange and hydrophobic effect drive the fiber formation, possibly through the formation of flip-flopped G-C18:1 dimers. These are not unexpected, as vesicle

membranes composed of G-C18:1 are interdigitated.[29,30] Flip-flopped dimers drive the morphological evolution at least until $[Ca^{2+}]/[G\text{-}C18:1]$ in the order of 0.5-0.6, that is until complete charge matching, according to *in situ* SAXS data.[43] A second step in the self-assembly of $\{Ca^{2+}\}$G-C18:1 occurs above a molar ratio of 0.6. The exothermic reaction probed by ITC must be understood in relationship to a ligand-ion binding,[103,107] probably driven by the proximity between COO^- and Ca^{2+} inside, but also, across the fibers, in analogy to the "egg-box" structures.[85,101] This is confirmed by the crystallization phenomenon above a ratio of 0.6 (but probably occurring at a lower ratio) shown by the *in situ* SAXS data.[43] It must be believed that the strong bidentate binding of carboxylate to calcium combined to the specific coordination geometry of the latter[111] and packing constraints of G-C18:1 drive the fibers' crystallization process. Crystallization could then be driven by a massive coordinating effect of calcium, as expected[111,112] and broadly found in many systems, including alginate.[101] The crystal structure is certainly associated to the fiber itself, although calcium-mediated coordination between fibers are also expected, as discussed further down. Nonetheless, this behavior seems to be peculiar only for G-C18:1, as no morphological changes are experienced by similar glycolipids (C18:1 sophorolipids, rhamnolipids) in solution when exposed to a calcium source.[116,117] Differently than silver, $\{Ca^{2+}\}$G-C18:1 materials are obtained through a continuous morphological evolution from micelles to fibers,[43] as also observed during the fibrillation of C16:0 sophorolipids.[68]

The complexity of the diffraction pattern in the SAXS profiles of $\{Ca^{2+}\}$G-C18:1 does not unfortunately provide a clear-cut answer about its crystal structure, but one can safely state that a 2D oblique lattice must be employed to account for the diffraction pattern (Figure S 2). We do suppose that the flip-flopped dimers constituting the oblique lattice are in the plane of the fiber, as shown in Figure 5a and as found for other cation-mediated fibrillar systems prepared under dilute conditions.[65,66] We do exclude the possibility of a ribbon phase, in which the oblique lattice would be orthogonal to the fiber's longitudinal axis (Figure S 2b), because this phase is generally observed for highly concentrated lyotropic liquid crystals,[63,64] while the G-C18:1 concentrations studied here are below 5 wt%. The approximate cross-section of the fibers is 10 nm, meaning that at least four G-C18:1 molecules are packed. All in all, calcium seems to play a double role, charge screening at low ion-to-lipid ratio, and coordinating ion at high ratio.

The sugar head group could also play an important role in the packing of G-C18:1. The first, crucial, role, concerns its hydrophilicity, which turns the oleic acid, C18:1, into a bolaform amphiphile. In the absence of glucose, one would expect the precipitation of a

crystal, as found for silver stearate.[95] In this regard, glucose not only contributes to the colloidal stability of the fibers in water, but, as discussed later, its bulkiness could also play a role in a defective side-by-side packing. The crucial role of glucose seems to be confirmed by the absence of morphological evolution when sister molecules like C18:1 sophorolipids (two glucose units) or rhamnolipids (a rhamnose unit) are studied in the presence of mono and divalent cations.[116,117]

On the other hand, conformation of the sugar head group in glycolipids has been reported to have a strong impact on the structure of their corresponding supramolecular aggregation.[118–120] The difference in terms of coordination geometry between silver and calcium, associated to a conformational effect of glucose could also explain the differences in terms of packing of the G-C18:1 in calcium and silver gels. In this regard, it is interesting to note that the twist along the fibers is much less obvious to observe in {Ca^{2+}}G-C18:1 than in sophorolipids,[50,62,68,121] thus indicating how the nanoscale ribbons found in the latter could be associated with the bulkiness of the sophorose group, compared to the glucose group in G-C18:1, as proposed elsewhere.[122]

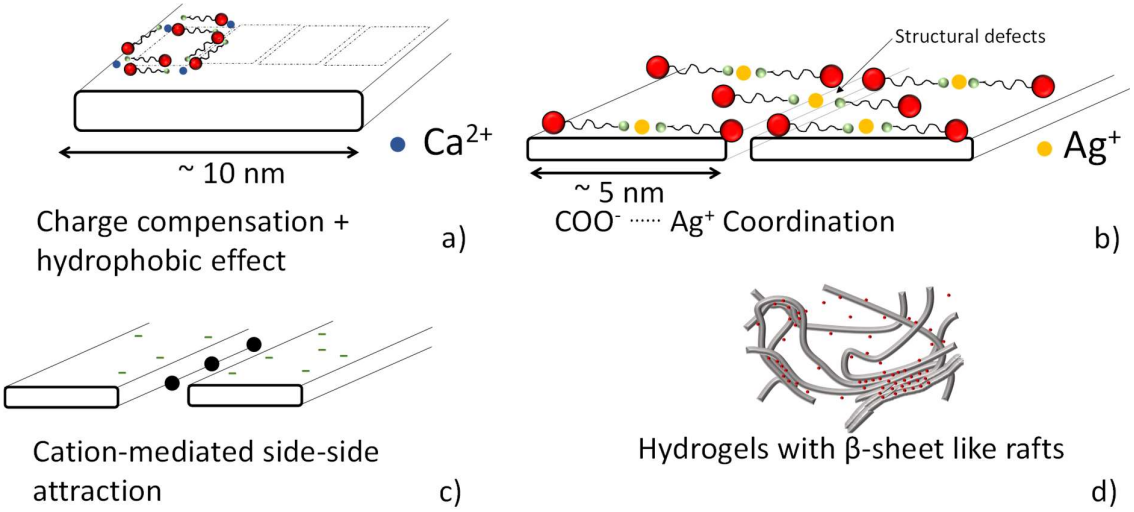

Figure 5 - Scheme of the possible hierarchical self-assembled structures found in a) {Ca^{2+}}G-C18:1 and b) {Ag^{+}}G-C18:1 gels. c) Illustration of the possible side-by-side, cation-mediated, interaction between {Ca^{2+}}G-C18:1 and {Ag^{+}}G-C18:1 fibers. d) "Nano fishnet" model structure of {Ca^{2+}}G-C18:1 and b) {Ag^{+}}G-C18:1 gels.

Lateral association into β-sheet-like rafts. The difference between hexagonal bundles and lamellar rafts lies in the anisotropy of the driving forces around each fiber. Previously reported cylindrical fibers, tubules or even flat fibers are generally described having an isotropic distribution of charges around the cross section, driving the system to the hexagonal

packing, the most energetically favorable structure for packed cylinders.[25,26] In the case of side-by-side interactions leading to multimers and raft, one must invoke the presence of an orientational force located at the external edge of the fibers, such as bridge-like cross-linking events driven by the cation, as found for alginate.[101] In the case of silver, the linear dimeric association of G-C18:1 results in the outward orientation of glucose at the side edges of the fibers. Directional side-by-side fiber attraction could then be driven by a number of phenomena, such as sugar-sugar interactions (hydrogen bonding, Van der Waals attraction) counterbalanced by repulsive short-range hydration forces[60,123] or cation-mediated interactions. In the latter, one could certainly suppose cation adsorption onto the neutral glucose layer, as recently reported for glycolipid membranes,[124] but, considering the strong exothermic heat exchange recorded for this system, silver-carboxylate coordination across adjacent fibers is still the most plausible hypothesis. In this regard, one must suppose the existence of structural flip-flop defects in the silver-G-C18:1 packing within the fiber plane, as proposed in Figure 5b. Flip-flop, which maximizes packing and minimizes repulsive steric interactions among sugar headgroups, was previously proposed in the case of interdigitated membranes composed of G-C18:1 and G-C18:0.[29,30,53] This hypothesis actually correlates well with the cryo-TEM data, which show a spurious connection between individual fibers, more compatible with a stochastic distribution of point defects than homogeneous interactions all along the fiber's length. Similar considerations hold for the calcium-based materials, with the main difference than the flip-flopped configuration of G-C18:1 inside the fiber probably introduces a more homogeneous negative charge density along the fiber's external sides. This could explain the cryo-TEM images, in which it is hard to observe individual fibers, which generally appear as dimers or, more often, multimers (Figure 2). Whether or not structural defects also characterize the molecular packing of $\{Ca^{2+}\}$G-C18:1 is impossible to affirm at the present state of the art. Although originating from a different packing of the G-C18:1, the overall cation-mediated mechanism of anisotropic attraction among fibers, resulting in the formation of β-sheet-like rafts, appears to be similar for both $\{Ca^{2+}\}$G-C18:1 and $\{Ag^{+}\}$G-C18:1 hydrogels (Figure 5c).

Hydrogel formation and stability. When lamellar rafts form, face-to-face dispersive forces should drive attraction between rafts and induce precipitation of lamellar crystals.[27,92] This does not seem to occur for $\{Ca^{2+}\}$G-C18:1 and $\{Ag^{+}\}$G-C18:1 hydrogels, in which SAFIN are relatively stable,[42] although this is not the case for other cation-driven G-C18:1 materials.[31] One must then suppose the presence of repulsive forces acting between the fibers'

faces. Hydration forces[123] are short-ranged (< 3 nm) and they are therefore excluded. Possible long-range repulsive forces could be attributed to electrostatic or steric interactions. Electrostatic forces could draw their origin from carboxylic groups oriented orthogonally to the fiber's plane. However, this hypothesis is highly unlikely for the number of structural considerations commented above. Condensation of ions, a well-known phenomenon in amphiphiles,[125–127] is a plausible mechanism considering the fact that the colloidal stability of the fibers and gel formation are not perturbed by excess ions ($[M^{z+}]/[G\text{-}C18:1] > 1$).[42] However, studying this mechanism would require a dedicated effort out of the scope of this work.

Helfrich undulations are an important long-range steric repulsive force found in lipid bilayer membranes and explaining the extreme swelling of lamellar phases.[128] Cryo-TEM (Figure 2) shows that the fibers, individual or associated, are flexible at scales above 100 nm. These undulations, with periods in the order of 200-500 nm, are compatible with the typical undulation wavelengths reported for swollen lamellar phases. Interestingly, neutron spin-echo experiments, commonly used to measure the stiffness of soft membranes,[129] run on the $\{Ca^{2+}\}$G-C18:1 fiber hydrogels (Figure 4a) show a slower decay of the spin echo intensity than in vesicles, with a $\frac{\Gamma_{ZG}}{q^3}$ (Eq. S2) about two orders of magnitude lower ($\sim 5 \cdot 10^{-2}$ nm^3/ns for vesicles against $\sim 1 \cdot 10^{-3}$ nm^3/ns for fibers). Since $\frac{\Gamma_{ZG}}{q^3}$ is inversely proportion to the bending rigidity (Eq. S3), NSE data confirms that fibers are more rigid than vesicles in the meso scale (4-8 nm), confirming the strong effect of Ca^{2+} on the collective dynamics of G-C18:1. A more quantitative analysis will be provided in future work.

If the hypothesis of undulation forces is not unreasonable, the rigidity of fibrillar $\{Ca^{2+}\}$G-C18:1 hydrogels must probably be compared to stiff lamellar L_β phases[130] than to swollen lamellar phases.[131] The different order between $\{Ca^{2+}\}$G-C18:1 fibers (crystalline) and G-C18:1 vesicle (liquid crystalline) could certainly explain the discrepancy and it should be said that we are not aware of bending rigidity studies on crystalline fibers using neutron spin echo so as to compare our data with. Further work could dissipate the present doubts.

Finally, although unlikely, one could invoke ligand stabilization effects of the fibers, where the ligand is G-C18:1 itself. Microbial glycolipids have a bolaform structure and they were shown to act as impressively good surface ligands for nanoparticles.[132] Hydrogels form above charge compensation and they are still stable in the excess of cations in solution. A fraction of G-C18:1 could then play a non-structural, passivating, role by screening the excess of charge on the fibers.

If the above shows that both Ca^{2+} and Ag^{+} play an important structural role in the fiber's formation and stability, with striking consequences on the elasticity and stability of the gels, complementary experiments show that their role is almost unique, if compared to other cations.[31] Alkaline earth, from Mg^{2+} to Ba^{2+}, but also as transition metals, like Fe^{2+}, Zn^{2+}, Mn^{2+} among others, can induce gelation[31] through a micelle-to-fiber transition.[43] However, the structure and morphology of the fibers, their size and aggregation state does not seem to be the same as the one found for {Ca^{2+}}G-C18:1 and {Ag^{+}}G-C18:1. In parallel, hydrogelation differs from cation to cation, it is either not induced or instantaneous but localized to the solution volume, where the ion solution is injected. We could find similar gelation with comparable structure of the fibers only with Mn^{2+} or Cr^{2+}, the latter most likely oxidized into Cr^{3+}. Cations can differ in size, charge density, polarizability, coordination sphere, reactivity, acido-basicity, just to cite some.[113–115] For this reason, a complete understanding of this new system would be challenging. Nonetheless, considering the pH-dependent speciation diagrams of each cation,[113] we found that hydrogels with lamellar raft domains are mostly observed for those cations which exist as free ions in solution in the pH range of hydrogel formation and which can adopt non-octahedral coordination, thus reinforcing the importance of the non-isotropic coordination by G-C18:1. More data and comments on these aspects are given in Ref. [31].

Conclusions

SAFiN from low molecular weight compounds commonly form hydrogels under dilute conditions, generally in the order of 1 wt% or less. Whatever the stimulus (temperature, pH, ionic strength) that drives fibrillation and consequent hydrogel formation, the structure of the gel is generally very similar across samples of different origin. SAFiN hydrogels are formed by an entangled network of infinitely long fibers. The typical X-ray or neutron scattering profiles display the form, and sometimes structure, a factor of individual fibers. In some specific cases, fibers form columnar structures (bundles) with a hexagonal order, driven by repulsive electrostatic interactions.

In this work, we report the unique "nano-fishnet" structure of self-assembled fibrillar hydrogels formed by metal-ligand complexes between Ca^{2+}, or Ag^{+}, ions and a natural glycolipid, G-C18:1. The gels display a combination of entanglement and β-sheet-like rafts. The "nano-fishnet" structure is not known for SAFiN hydrogels but generally found for more complex aminoacid-based systems, like natural actin and silk proteins.

G-C18:1 is a new bolaform glucolipid containing a free-standing COOH group and belonging to the broad family of biological amphiphiles (biosurfactants). In its micellar phase at pH above neutrality, the addition of a Ca^{2+} or Ag^{+} solution drives a micelle-to-fiber phase transition, not expected for specific compound, it rather forms interdigitated membrane vesicles in its neutral form at pH below neutrality. Fibers have an approximate cross-section of 10 and 5 nm, respectively for {Ca^{2+}}G-C18:1 and {Ag^{+}}G-C18:1 systems. Above about 0.5 wt%, the addition of the ion solution also drives the formation of a hydrogel, of which the strength is maximized at a stoichiometric negative/positive charge ratio between the COO^{-} group of the glucolipid and the cation. The gel strength (G´) increases with glucolipid concentration according to a power law dependency in the order of 2.3-2.6. The strength of the hydrogels is one order of magnitude higher for {Ag^{+}}G-C18:1 with respect to {Ca^{2+}}G-C18:1 and so is the stability against shearing and temperature, shown elsewhere.[42]

{Ag^{+}}G-C18:1 hydrogels display a long-range lamellar order of the fibers, systematically observed at rest, independently of shear, heating or combination of both.[42] Such order is observed both by cryo-TEM, showing how individual fibers spontaneously assemble into lamellar multimers, and, above all, SAXS. Similar results are also observed for {Ca^{2+}}G-C18:1 hydrogels, although the lamellar structure factor is partially or totally lost when hydrogels are sheared.

The structural SAXS and cryo-TEM data prone for a β-sheet-like raft structure of both {Ca^{2+}}G-C18:1 and {Ag^{+}}G-C18:1 hydrogels up to at least 5 wt% of glucolipid in solution. The strong stability towards shear and temperature can probably be explained by such β-sheet-like structure, in analogy to silk fibroin, of which the hydrogels are also very stable.

The main hypothesis explaining the existence of β-sheet-like rafts concerns the anisotropic distribution of negative charges in the fibers, most likely located on the fibers alongside. The counterions would then act as “glue” across adjacent fibers through charge-screening or coordination interactions. Isothermal titration calorimetry partly corroborates this hypothesis, as it shows a strong exothermic signal, typical for specific interactions, when cations are added to the solution. However, ITC, combined with complementary ion-resolved *in situ* SAXS experiments presented elsewhere,[43] also shows important differences between the calcium and silver systems. In {Ca^{2+}}G-C18:1, negatively charged G-C18:1 micelles undergo a continuous micelle-to-fiber morphological transition with two well-identified steps: low calcium content (< 0.3 molar ratio) favors the micelle-to-fiber transition, while high calcium concentration (> 0.3 molar ratio) favors fiber crystallization. In {Ag^{+}}G-C18:1, negatively-charged micelles serve as a reservoir of matter for G-C18:1 molecules: silver ions

immediately react with G-C18:1 to form dimers, which promptly associate into fibers. We believe that structural defects in packing of G-C18:1 are responsible for the spurious accumulation of negative charges on the fibers alongside, thus driving raft formation mediated by the free cations in solution.

Acknowledgements

We thank Dr. S. Roelants at Gent University and Bio Base Europe Pilot Plant, Gent, Belgium for dealing with and shipping the G-C18:1 glycolipid. Authors kindly acknowledge the French ANR, Project N° SELFAMPHI - 19-CE43-0012-01. Soleil synchrotron is acknowledged for financial support during the beamtime associated to the proposal number N°20201747. ESRF synchrotron is acknowledged for financial support during the beamtime associated to the proposal numbers N°MX 2311. Laurent Michot (Sorbonne Université, Paris, France) is kindly acknowledged for sharing the beamtime (Proposal N°: BAG 20201118) on the SWING beamline at Soleil synchrotron, Saint-Aubin, France. Marianne Impéror-Clerc (Université Paris-Saclay, France) is acknowledged for helpful discussions. This work has been sponsored by the Ile-de-France Region in the framework of the DIM Respore, the Ile-de-France network of Excellence in Porous Solids. Raw data from NSE measurements is available under dx.doi.org/10.5291/ILL-DATA.9-13-915.

References

1. Raghavan, S. R. & Douglas, J. F. The conundrum of gel formation by molecular nanofibers, wormlike micelles, and filamentous proteins: gelation without cross-links? *Soft Matter* **8**, 8539 (2012).
2. Ahsan, A., Tian, W. X., Farooq, M. A. & Khan, D. H. An overview of hydrogels and their role in transdermal drug delivery. *Int. J. Polym. Mater. Polym. Biomater.* **0**, 1–11 (2020).
3. Wichterle, O. & Lim, D. Hydrophilic Gels for Biological Use. *Nature* **185**, 117–118 (1960).
4. Van Vlierberghe, S., Dubruel, P. & Schacht, E. Biopolymer-based hydrogels as scaffolds for tissue engineering applications: A review. *Biomacromolecules* **12**, 1387–1408 (2011).
5. Tam, A. Y. Y. & Yam, V. W. W. Recent advances in metallogels. *Chem. Soc. Rev.* **42**, 1540–1567 (2013).

6. Piepenbrock, M. M., Lloyd, G. O., Clarke, N. & Steed, J. W. Metal- and Anion-Binding Supramolecular Gels. 1960–2004 (2010).
7. Draper, E. R. *et al.* Opening a Can of Worm(-like Micelle)s: The Effect of Temperature of Solutions of Functionalized Dipeptides. *Angew. Chemie* **129**, 10603–10606 (2017).
8. Adams, D. J. *et al.* A new method for maintaining homogeneity during liquid-hydrogel transitions using low molecular weight hydrogelators. *Soft Matter* **5**, 1856–1862 (2009).
9. Carretti, E. *et al.* Structure and rheology of gel nanostructures from a vitamin C-based surfactant. *Phys. Chem. Chem. Phys.* **18**, 8865–8873 (2016).
10. Draper, E. R. & Adams, D. J. Low-Molecular-Weight Gels: The State of the Art. *Chem* **3**, 390–410 (2017).
11. Yu, G., Yan, X., Han, C. & Huang, F. Characterization of supramolecular gels. *Chem. Soc. Rev.* **42**, 6697–6722 (2013).
12. Rathore, O. & Sogah, D. Y. Nanostructure formation through β-sheet self-assembly in silk-based materials. *Macromolecules* **34**, 1477–1486 (2001).
13. Fink, T. D. & Zha, R. H. Silk and Silk-Like Supramolecular Materials. *Macromol. Rapid Commun.* **39**, 1–17 (2018).
14. Kim, U. J. *et al.* Structure and properties of silk hydrogels. *Biomacromolecules* **5**, 786–792 (2004).
15. Liu, R. *et al.* "Nano-Fishnet" Structure Making Silk Fibers Tougher. *Adv. Funct. Mater.* **26**, 5534–5541 (2016).
16. Gardel, M. L. *et al.* Elastic behavior of cross-linked and bundled actin networks. *Science (80-.).* **304**, 1301–1305 (2004).
17. Pelletier, O. *et al.* Structure of actin cross-linked with [formula presented]-actinin: A network of bundles. *Phys. Rev. Lett.* **91**, 3–6 (2003).
18. Wong, G. C. L. *et al.* Lamellar Phase of Stacked Two-Dimensional Rafts of Actin Filaments. *Phys. Rev. Lett.* **91**, 1–4 (2003).
19. Ochi, A., Hossain, K. S., Ooyama, E., Magoshi, J. & Nemoto, N. Dynamic light scattering of native silk fibroin solution extracted from different parts of the middle division of the silk gland of the Bombyx mori silkworm. *Biomacromolecules* **4**, 350–359 (2003).
20. Calabrese, V. *et al.* Understanding heat driven gelation of anionic cellulose nanofibrils: Combining saturation transfer difference (STD) NMR, small angle X-ray scattering (SAXS) and rheology. *J. Colloid Interface Sci.* **535**, 205–213 (2019).

21. Okesola, B. O. *et al.* Supramolecular Self-Assembly to Control Structural and Biological Properties of Multicomponent Hydrogels. *Chem. Mater.* **31**, 7883–7897 (2019).
22. Yu, Z., Tantakitti, F., Palmer, L. C. & Stupp, S. I. Asymmetric Peptide Nanoribbons. *Nano Lett.* **16**, 6967–6974 (2016).
23. Draper, E. R. *et al.* Using Small-Angle Scattering and Contrast Matching to Understand Molecular Packing in Low Molecular Weight Gels. *Matter* **2**, 764–778 (2020).
24. McAulay, K. *et al.* Isotopic Control over Self-Assembly in Supramolecular Gels. *Langmuir* **36**, 8626–8631 (2020).
25. Terech, P. & Maitra, U. Structural and rheological properties of aqueous viscoelastic solutions and gels of tripodal cholamide-based self-assembled supramolecules. *J. Phys. Chem. B* **112**, 13483–13492 (2008).
26. Cui, H. *et al.* Spontaneous and X-ray–Triggered Crystallization at Long Range in Self-Assembling Filament Networks. *Science (80-.).* **327**, 555–560 (2010).
27. Weingarten, A. S. *et al.* Self-assembling hydrogel scaffolds for photocatalytic hydrogen production. *Nat. Chem.* **6**, 964–970 (2014).
28. Baccile, N. *et al.* Chameleonic Amphiphile: the Unique Multiple Self-Assembly Properties of a Natural Glycolipid in Excess of Water. *Submitted* https://hal.archives-ouvertes.fr/hal-03576358 (2022).
29. Baccile, N. *et al.* PH-Driven Self-Assembly of Acidic Microbial Glycolipids. *Langmuir* **32**, 6343–6359 (2016).
30. Baccile, N. *et al.* Self-Assembly Mechanism of pH-Responsive Glycolipids: Micelles, Fibers, Vesicles, and Bilayers. *Langmuir* **32**, 10881–10894 (2016).
31. Poirier, A. *et al.* Metallogels from glycolipid biosurfactant. *Submitted* https://hal.archives-ouvertes.fr/hal-03576357v1 (2022).
32. Angelescu, D., Caldararu, H. & Khan, A. Some observations on the effect of the trivalent counterion Al3+ to the self-assembly of sodium dodecyl sulphate in water. *Colloids Surfaces A Physicochem. Eng. Asp.* **245**, 49–60 (2004).
33. Vasilescu, M., Angelescu, D., Caldararu, H., Almgren, M. & Khan, A. Fluorescence study on the size and shape of sodium dodecyl sulphate-aluminium salt micelles. *Colloids Surfaces A Physicochem. Eng. Asp.* **235**, 57–64 (2004).
34. Srinivasan, V. & Blankschtein, D. Effect of Counterion Binding on Micellar Solution Behavior: 2. Prediction of Micellar Solution Properties of Ionic Surfactant-Electrolyte

Systems. *Langmuir* **19**, 9946–9961 (2003).

35. Qiao, Y., Lin, Y., Wang, Y., Li, Z. & Huang, J. Metal-driven viscoelastic wormlike micelle in anionic/zwitterionic surfactant systems and template-directed synthesis of dendritic silver nanostructures. *Langmuir* **27**, 1718–1723 (2011).
36. Guo, J. *et al.* Switchable Supramolecular Configurations of Al3+/LysTPY Coordination Polymers in a Hydrogel Network Controlled by Ultrasound and Heat. *ACS Appl. Mater. Interfaces* **13**, 40079–40087 (2021).
37. Chen, L., McDonald, T. O. & Adams, D. J. Salt-induced hydrogels from functionalised-dipeptides. *RSC Adv.* **3**, 8714–8720 (2013).
38. Zhou, X. R., Ge, R. & Luo, S. Z. Self-assembly of pH and calcium dual-responsive peptide-amphiphilic hydrogel. *J. Pept. Sci.* **19**, 737–744 (2013).
39. Xie, Y. *et al.* Calcium-Ion-Triggered Co-assembly of Peptide and Polysaccharide into a Hybrid Hydrogel for Drug Delivery. *Nanoscale Res. Lett.* **11**, (2016).
40. Greenfield, M. A., Hoffman, J. R., De La Cruz, M. O. & Stupp, S. I. Tunable mechanics of peptide nanofiber gels. *Langmuir* **26**, 3641–3647 (2010).
41. Shi, J., Gao, Y., Zhang, Y., Pan, Y. & Xu, B. Calcium ions to cross-link supramolecular nanofibers to tune the elasticity of hydrogels over orders of magnitude. *Langmuir* **27**, 14425–14431 (2011).
42. Poirier, A., Bizien, T., Zinn, T., Pernot, P. & Baccile, N. Self-assembled fibrillar network (SAFiN) hydrogels with β-sheet-like domains: Properties. *Submitted* https://hal.archives-ouvertes.fr/hal-03576363v1 (2022).
43. Poirier, A., Griel, P. Le, Perez, J. & Baccile, N. Cation-induced fibrillation of microbial glycolipid probed by ion-resolved in situ SAXS. *Submitted* https://hal.archives-ouvertes.fr/hal-03576366v1 (2022).
44. Saerens, K. M. J., Zhang, J., Saey, L., Van Bogaert, I. N. A. & Soetaert, W. Cloning and functional characterization of the UDP-glucosyltransferase UgtB1 involved in sophorolipid production by Candida bombicola and creation of a glucolipid-producing yeast strain. *Yeast* **28**, 279–292 (2011).
45. Seyrig, C. *et al.* Stimuli-induced non-equilibrium phase transitions in polyelectrolyte-surfactant complex coacervates. *Langmuir* **36**, 8839–8857 (2020).
46. Renterghem, L. Van *et al.* Easy Formation of Functional Liposomes in Water Using a pH-Responsive Microbial Glycolipid: Encapsulation of Magnetic and Upconverting Nanoparticles. *ChemNanoMat* **5**, 1188–1201 (2019).
47. Song, A. & Hao, J. Self-assembly of metal-ligand coordinated charged vesicles. *Curr.*

Opin. Colloid Interface Sci. **14**, 94–102 (2009).

48. De Gennes, P.-G. Dynamics of Entangled Polymer Solutions. I. The Rouse Model. *Macromolecules* **9**, 587–593 (1976).
49. Chen, S. Q., Lopez-Sanchez, P., Wang, D., Mikkelsen, D. & Gidley, M. J. Mechanical properties of bacterial cellulose synthesised by diverse strains of the genus Komagataeibacter. *Food Hydrocoll.* **81**, 87–95 (2018).
50. Baccile, N. *et al.* Bio-based glyco-bolaamphiphile forms a temperature-responsive hydrogel with tunable elastic properties. *Soft Matter* **14**, 7859–7872 (2018).
51. Gradzielski, M. Vesicles and vesicle gels — structure and dynamics of formation. *J. Phys. Condens. Matter* **15**, R655 (2003).
52. Warriner, H. E., Idziak, S. H., Slack, N. L., Davidson, P. & Safinya, C. R. Lamellar biogels: fluid-membrane-based hydrogels containing polymer lipids. *Science (80-.).* **271**, 969–73 (1996).
53. Ben Messaoud, G. *et al.* Single-Molecule Lamellar Hydrogels from Bolaform Microbial Glucolipids. *Soft Matter* **16**, 2528–2539 (2020).
54. Leontidis, E. Investigations of the Hofmeister series and other specific ion effects using lipid model systems. *Adv. Colloid Interface Sci.* **243**, 8–22 (2017).
55. Ji, S., Xu, L., Fu, X., Sun, J. & Li, Z. Light- and Metal Ion-Induced Self-Assembly and Reassembly Based on Block Copolymers Containing a Photoresponsive Polypeptide Segment. *Macromolecules* **52**, 4686–4693 (2019).
56. Chen, L. *et al.* Salt-induced hydrogelation of functionalised-dipeptides at high pH. *Chem. Commun.* **47**, 12071–12073 (2011).
57. Cardoso, A. Z. *et al.* Linking micellar structures to hydrogelation for salt-triggered dipeptide gelators. *Soft Matter* **12**, 3612–3621 (2016).
58. Çelik, E., Bayram, C., Akçapinar, R., Türk, M. & Denkbaş, E. B. The effect of calcium chloride concentration on alginate/Fmoc-diphenylalanine hydrogel networks. *Mater. Sci. Eng. C* **66**, 221–229 (2016).
59. Paineau, E. *et al.* Role of initial precursors on the liquid-crystalline phase behavior of synthetic aluminogermanate imogolite nanotubes. *J. Colloid Interface Sci.* **580**, 275–285 (2020).
60. Baccile, N. & Cristiglio, V. Primary and Secondary Hydration Forces between Interdigitated Membranes Composed of Bolaform Microbial Glucolipids. *Langmuir* **36**, 2191–2198 (2020).
61. Cui, H., Muraoka, T., Cheetham, A. G. & Stupp, S. I. Self-Assembly of Giant Peptide

Nanobelts. *Nano Lett.* **9**, 945–951 (2009).

62. Cuvier, A.-S. S. *et al.* pH-triggered formation of nanoribbons from yeast-derived glycolipid biosurfactants. *Soft Matter* **10**, 3950–3959 (2014).
63. Lis, L. J., Quinn, P. J. & Collins, J. M. Structures and Mechanisms of Phase Transitions in Surfactant Mixtures: Systems Which Induce the Ribbon Phase. *Mol. Cryst. Liq. Cryst. Inc. Nonlinear Opt.* **170**, 119–133 (1989).
64. Hyde, S. T. Identification of Lyotropic Liquid Crystalline Mesophases. in *Handbook ofApplied Surface and Colloid Chemistry.* (ed. Holmberg, K.) 299 (John Wiley & Sons, Ltd, 2001). doi:10.1002/asna.18730821002.
65. Qiao, Y. *et al.* Metal-Driven Hierarchical Self-Assembled One-Dimensional Nanohelices. *Nano Lett.* **9**, 4500–4504 (2009).
66. Oda, R., Artzner, F., Laguerre, M. & Huc, I. Molecular structure of self-assembled chiral nanoribbons and nanotubules revealed in the hydrated state. *J. Am. Chem. Soc.* **130**, 14705–14712 (2008).
67. Masuda, M. & Shimizu, T. Lipid nanotubes and microtubes: Experimental evidence for unsymmetrical monolayer membrane formation from unsymmetrical bolaamphiphiles. *Langmuir* **20**, 5969–5977 (2004).
68. Baccile, N. *et al.* Palmitic Acid Sophorolipid Biosurfactant: From Self-Assembled Fibrillar Network (SAFiN) To Hydrogels with Fast Recovery. *Philos. Trans. A* **379**, 20200343 (2021).
69. Greaves, T. L. *et al.* How ionic species structure influences phase structure and transitions from protic ionic liquids to liquid crystals to crystals. *Faraday Discuss.* **206**, 29–48 (2018).
70. Mannock, D. A. *et al.* The thermotropic phase behaviour and phase structure of a homologous series of racemic β-d-galactosyl dialkylglycerols studied by differential scanning calorimetry and X-ray diffraction. *Chem. Phys. Lipids* **148**, 26–50 (2007).
71. Teixeira, J. Small-angle scattering by fractal systems. *J. Appl. Crystallogr.* **21**, 781–785 (1988).
72. Moyer, T. J., Cui, H. & Stupp, S. I. Tuning nanostructure dimensions with supramolecular twisting. *J. Phys. Chem. B* **117**, 4604–4610 (2013).
73. Adamcik, J. *et al.* Microtubule-Binding R3 Fragment from Tau Self-Assembles into Giant Multistranded Amyloid Ribbons. *Angew. Chemie - Int. Ed.* **55**, 618–622 (2016).
74. Raghavan, S. R. Distinct character of surfactant gels: A smooth progression from micelles to fibrillar networks. *Langmuir* **25**, 8382–8385 (2009).

75. Pomerantz, W. C. *et al.* Nanofibers and lyotropic liquid crystals from a class of self-assembling β-peptides. *Angew. Chemie - Int. Ed.* **47**, 1241–1244 (2008).
76. Ben Messaoud, G. *et al.* pH-controlled self-assembled fibrillar network (SAFiN) hydrogels: evidence of a kinetic control of the mechanical properties. *Chem. Mater.* **31**, 4817–4830 (2019).
77. Kim, J., Park, C. H., Kim, S. H., Yoon, S. & Piao, L. Mechanism of organogel formation from mixed-ligand silver (I) carboxylates. *Bull. Korean Chem. Soc.* **32**, 3267–3273 (2011).
78. Westcott, A., Sumby, C. J., Walshaw, R. D. & Hardie, M. J. Metallo-gels and organo-gels with tripodal cyclotriveratrylene-type and 1,3,5-substituted benzene-type ligands. *New J. Chem.* **33**, 902–912 (2009).
79. Wei, T. *et al.* Novel smart supramolecular metallo-hydrogel that could selectively recognize and effectively remove Pb2+ in aqueous solution. *Sci. China Chem.* **55**, 2554–2561 (2012).
80. Shao, T., Falcone, N. & Kraatz, H. B. Supramolecular Peptide Gels: Influencing Properties by Metal Ion Coordination and Their Wide-Ranging Applications. *ACS Omega* **5**, 1312–1317 (2020).
81. Li, H., Yang, P., Pageni, P. & Tang, C. Recent Advances in Metal-Containing Polymer Hydrogels. *Macromol. Rapid Commun.* **38**, 1–9 (2017).
82. Maire du Poset, A., Zitolo, A., Cousin, F., Assifaoui, A. & Lerbret, A. Evidence for an egg-box-like structure in iron(II)-polygalacturonate hydrogels: a combined EXAFS and molecular dynamics simulation study. *Phys. Chem. Chem. Phys.* **2019-Novem**, (2019).
83. Maire Du Poset, A. *et al.* Tuning the Structure of Galacturonate Hydrogels: External Gelation by Ca, Zn, or Fe Cationic Cross-Linkers. *Biomacromolecules* **20**, 2864–2872 (2019).
84. Huynh, U. T. D., Lerbret, A., Neiers, F., Chambin, O. & Assifaoui, A. Binding of Divalent Cations to Polygalacturonate: A Mechanism Driven by the Hydration Water. *J. Phys. Chem. B* **120**, 1021–1032 (2016).
85. Assifaoui, A. *et al.* Structural behaviour differences in low methoxy pectin solutions in the presence of divalent cations (Ca2+and Zn2+): A process driven by the binding mechanism of the cation with the galacturonate unit. *Soft Matter* **11**, 551–560 (2015).
86. Shi, J. H., Liu, X. Y., Li, J. L., Strom, C. S. & Xu, H. Y. Spherulitic networks: From structure to rheological property. *J. Phys. Chem. B* **113**, 4549–4554 (2009).
87. Chen, L. *et al.* Tuneable mechanical properties in low molecular weight gels. *Soft*

Matter **7**, 9721 (2011).

88. Wang, R. Y., Liu, X. Y., Narayanan, J., Xiong, J. Y. & Li, J. L. Architecture of fiber network: From understanding to engineering of molecular gels. *J. Phys. Chem. B* **110**, 25797–25802 (2006).
89. Cui, H., Cheetham, A. G., Newcomb, C. J. & Stupp, S. I. Self-Assembling Filament Networks. *Science (80-.).* **555**, 555–560 (2010).
90. Needleman, D. J. *et al.* Higher-order assembly of microtubules by counterions: From hexagonal bundles to living necklaces. *Proc. Natl. Acad. Sci. U. S. A.* **101**, 16099–16103 (2004).
91. Safinya, C. R. *et al.* Nanoscale assembly in biological systems: From neuronal cytoskeletal proteins to curvature stabilizing lipids. *Adv. Mater.* **23**, 2260–2270 (2011).
92. Zhang, S. *et al.* A self-assembly pathway to aligned monodomain gels. *Nat. Mater.* **9**, 594–601 (2010).
93. Vand, V., Aitken, A. & Campbell, R. K. Crystal structure of silver salts of fatty acids. *Acta Crystallogr.* **2**, 398–403 (1949).
94. Smith, G. *et al.* Structures of the silver (I) complexes with maleic and fumaric acids: Silver(I) hydrogen maleate, silver(I) maleate and silver (I) fumarate. *Zeitschrift fur Krist. - New Cryst. Struct.* **210**, 44–48 (1995).
95. Tolochko, B. P., Chernov, S. V., Nikitenko, S. G. & Whitcomb, D. R. EXAFS determination of the structure of silver stearate, [Ag(O2C(CH2)16CH3]2, and the effect of temperature on the silver coordination sphere. *Nucl. Instruments Methods Phys. Res. Sect. A Accel. Spectrometers, Detect. Assoc. Equip.* **405**, 428–434 (1998).
96. Bairi, P., Roy, B. & Nandi, A. K. PH and anion sensitive silver(i) coordinated melamine hydrogel with dye absorbing properties: Metastability at low melamine concentration. *J. Mater. Chem.* **21**, 11747–11749 (2011).
97. Xu, F. *et al.* Synthesis and properties of the metallo-supramolecular polymer hydrogel poly[methyl vinyl ether-alt-mono-sodium maleate]·AgNO3: Ag+/Cu2+ ion exchange and effective antibacterial activity. *J. Mater. Chem. B* **2**, 6406–6411 (2014).
98. Liu, Y. *et al.* Silver(i)-glutathione biocoordination polymer hydrogel: Effective antibacterial activity and improved cytocompatibility. *J. Mater. Chem.* **21**, 19214–19218 (2011).
99. Chiad, K. *et al.* Isothermal titration calorimetry: A powerful technique to quantify interactions in polymer hybrid systems. *Macromolecules* **42**, 7545–7552 (2009).
100. Brautigam, C. A. Fitting two- and three-site binding models to isothermal titration

calorimetric data. *Methods* **76**, 124–136 (2015).

101. Fang, Y. *et al.* Multiple steps and critical behaviors of the binding of calcium to alginate. *J. Phys. Chem. B* **111**, 2456–2462 (2007).
102. Loh, W., Brinatti, C. & Tam, K. C. Use of isothermal titration calorimetry to study surfactant aggregation in colloidal systems. *Biochim. Biophys. Acta - Gen. Subj.* **1860**, 999–1016 (2016).
103. Sinn, C. G., Dimova, R. & Antonietti, M. Isothermal titration calorimetry of the polyelectrolyte/water interaction and binding of Ca2+: Effects determining the quality of polymeric scale inhibitors. *Macromolecules* **37**, 3444–3450 (2004).
104. Lehrmann, R. & Seelig, J. Adsorption of Ca2+ and La3+ to bilayer membranes: Measurement of the adsorption enthalpy and binding constant with titration calorimetry. *BBA - Biomembr.* **1189**, 89–95 (1994).
105. Du, C. *et al.* Thermodynamics of mixed surfactant solutions of N, N ′-bis(dimethyldodecyl)-1,2-ethanediammoniumdibromide with 1-dodecyl-3-methylimidazolium bromide. *J. Phys. Chem. B* **118**, 1168–1179 (2014).
106. Ito, T. H., Rodrigues, R. K., Loh, W. & Sabadini, E. Calorimetric and Light Scattering Investigations of the Transition from Spherical to Wormlike Micelles of C14TAB Triggered by Salicylate. *Langmuir* **31**, 6020–6026 (2015).
107. Johnson, R. A., Manley, O. M., Spuches, A. M. & Grossoehme, N. E. Dissecting ITC data of metal ions binding to ligands and proteins. *Biochim. Biophys. Acta - Gen. Subj.* **1860**, 999–1016 (2016).
108. Löf, D., Niemiec, A., Schillén, K., Loh, W. & Olofsson, G. A calorimetry and light scattering study of the formation and shape transition of mixed micelles of EO20PO68EO20 triblock copolymer (P123) and nonionic surfactant (C12EO6). *J. Phys. Chem. B* **111**, 5911–5920 (2007).
109. Bastos-González, D., Pérez-Fuentes, L., Drummond, C. & Faraudo, J. Ions at interfaces: The central role of hydration and hydrophobicity. *Curr. Opin. Colloid Interface Sci.* **23**, 19–28 (2016).
110. Ringbom, A. *Complexation in Analytical Chemistry*. (John Wiley & Sons, Inc., 1963).
111. Katz, A. K., Glusker, J. P., Beebe, S. A. & Bock, C. W. Calcium ion coordination: A comparison with that of beryllium, magnesium, and zinc. *J. Am. Chem. Soc.* **118**, 5752–5763 (1996).
112. Carrell, C. J., Carrell, H. L., Erlebacher, J. & Glusker, J. P. Structural Aspects of Metal Ion-Carboxylate Interactions. *J. Am. Chem. Soc.* **110**, 8651–8656 (1988).

113. Baes, C. F. & Mesmer, R. E. *The Hydrolysis of Cations*. (John Wiley & Sons, Inc., 1976).
114. Lincoln, S. F., Richens, D. T. & Sykes, A. G. Metal Aqua Ions. in *Comprehensive Coordination Chemistry II* 515–555 (2003).
115. Persson, I. Hydrated metal ions in aqueous solution: How regular are their structures? *Pure Appl. Chem.* **82**, 1901–1917 (2010).
116. Baccile, N., Pedersen, J. S., Pehau-Arnaudet, G. & Van Bogaert, I. N. a. Surface charge of acidic sophorolipid micelles: effect of base and time. *Soft Matter* **9**, 4911–4922 (2013).
117. Chen, M. *et al.* Influence of calcium ions on rhamnolipid and rhamnolipid/anionic surfactant adsorption and self-assembly. *Langmuir* **29**, 3912–3923 (2013).
118. Svenson, S., Kirste, B. & Fuhrhop, J. H. A CPMAS 13C NMR Study of Molecular Conformations and Disorder of N-Octylhexonamides in Microcrystals and Supramolecular Assemblies. *J. Am. Chem. Soc.* **116**, 11969–11975 (1994).
119. Svenson, S., Schaefer, A. & Fuhrhop, J. H. Conformational Effects of 1.3-syn-Diaxial Repulsion and 1.2-gauche Attraction Between Hydroxy Groups n Monomolecula r N-Octyl-D-hexonamide Solutions A 13C and ’H NMR Spectroscopic Study Sonke. *J. Chem. Soc. Perkin Trans. 2* **2**, 1023–1028 (1994).
120. Svenson, S., Koening, J. & Fuhrhop, J. H. Crystalline Order in Probably Hollow Micellar Fibers of N-Octyl-D-gluconamide. *J. Phys. Chem.* **98**, 1022–1028 (1994).
121. Cuvier, A. S. *et al.* Synthesis of Uniform, Monodisperse, Sophorolipid Twisted Ribbons. *Chem. - An Asian J.* **10**, 2419–2426 (2015).
122. Barclay, T. G., Constantopoulos, K. & Matisons, J. Nanotubes self-assembled from amphiphilic molecules via helical intermediates. *Chem. Rev.* **114**, 10217–10291 (2014).
123. Parsegian, V. A. & Zemb, T. Hydration forces: Observations, explanations, expectations, questions. *Curr. Opin. Colloid Interface Sci.* **16**, 618–624 (2011).
124. Stefaniu, C. *et al.* Headgroup-Ordered Monolayers of Uncharged Glycolipids Exhibit Selective Interactions with Ions. *J. Phys. Chem. Lett.* **10**, 1684–1690 (2019).
125. Dvir, T. *et al.* Charged membranes under confinement induced by polymer-, salt-, or ionic liquid solutions. *Soft Matter* **9**, 10640 (2013).
126. Lotan, O., Fink, L., Shemesh, A., Tamburu, C. & Raviv, U. Critical Conditions for Adsorption of Calcium Ions onto Dipolar Lipid Membranes. *J. Phys. Chem. A* **120**, 3390–3396 (2016).
127. Yaghmur, A., Laggner, P., Sartori, B. & Rappolt, M. Calcium triggered Lα-H2 phase

transition monitored by combined rapid mixing and time-resolved synchrotron SAXS. *PLoS One* **3**, (2008).

128. Helfrich, W. Steric Interaction of Fluid Membranes in Multilayer Systems. *Z. Naturforsch* **33a**, 305–315 (1978).
129. Monzel, C. & Sengupta, K. Measuring shape fluctuations in biological membranes. *J. Phys. D. Appl. Phys.* **49**, 243002 (2016).
130. Gupta, S., Mel, J. U. De & Schneider, G. J. Dynamics of liposomes in the fluid phase. *Curr. Opin. Colloid Interface Sci.* **42**, 121 (2019).
131. Nagao, M., Chawang, S. & Hawa, T. Interlayer distance dependence of thickness fluctuations in a swollen lamellar phase. *Soft Matter* **7**, 6598–6605 (2011).
132. Lassenberger, A. *et al.* Biocompatible Glyconanoparticles by Grafting of Sophorolipid Monolayers on Monodisperse Iron Oxide Nanoparticles. *ACS Appl. Bio Mater.* **2**, 3095–3107 (2019).